BIOCHEMISTRY
including biophysical chemistry & molecular biology
Article

*Biochemistry* **2009,** *48,* 7575–7583 7575
DOI: 10.1021/bi900769j

# The Hypervariable Region of K-Ras4B Is Responsible for Its Specific Interactions with Calmodulin†

Sherwin J. Abraham,‡ Ryan P. Nolet,‡ Richard J. Calvert,§,∥ Lucy M. Anderson,§ and Vadim Gaponenko*,‡

‡*Department of Biochemistry and Molecular Genetics, University of Illinois, Chicago, Illinois 60607,* §*Laboratory of Comparative Carcinogenesis, National Cancer Institute, Frederick, Maryland 21702, and*∥ *Division of Bioanalytical Chemistry, U.S. Food and Drug Administration, College Park, Maryland 20740*

*Received May 5, 2009; Revised Manuscript Received June 30, 2009*

ABSTRACT: K-Ras4B belongs to the family of p21 Ras GTPases, which play an important role in cell proliferation, survival, and motility. The p21 Ras proteins, such as K-Ras4B, K-Ras4A, H-Ras, and N-Ras, share 85% sequence homology and activate very similar signaling pathways. Only the C-terminal hypervariable regions differ significantly. A growing body of literature demonstrates that each Ras isoform possesses unique functions in normal physiological processes as well as in pathogenesis. One of the central questions in the field of Ras biology is how these very similar proteins achieve such remarkable specificity in protein−protein interactions that regulate signal transduction pathways. Here we explore specific binding of K-Ras4B to calmodulin. Using NMR techniques and isothermal titration calorimetry, we demonstrate that the hypervariable region of K-Ras4B contributes in a major way to the interaction with calmodulin, while the catalytic domain of K-Ras4B provides a way to control the interaction by nucleotide binding. The hypervariable region of K-Ras4B binds specifically to the C-terminal domain of $Ca^{2+}$-loaded calmodulin with micromolar affinity, while the GTP-$\gamma$-S-loaded catalytic domain of K-Ras4B may interact with the N-terminal domain of calmodulin.

Members of the Ras family of proto-oncogenes are mutated in up to a third of human malignancies (*1*, *2*). These are small p21 GTPases that cycle between the GDP-bound inactive and the GTP-bound active states to transmit intracellular signals. How Ras proteins contribute to cancer development is not fully understood, in spite of much study. They have many signaling partners and regulate a variety of cellular processes including proliferation, transformation, differentiation, metastasis, and apoptosis. There are four isoforms in the Ras family, and of these K-Ras, almost exclusively, is mutated in common epithelial cancers including those of the pancreas, colon, and lung. Two forms of K-Ras are generated by alternate mRNA splicing, namely, K-Ras4A and K-Ras4B. K-Ras4B is more abundant in most tissues and has been demonstrated to cause tumor formation in studies with genetically engineered mice (*3*−*5*). Noonan syndrome, a developmental disorder, is caused by a mutation specifically in K-Ras4B (*6*).

Thus, K-Ras4B has a particularly important role in human cancer as well as human development. It differs from the other highly homologous Ras isoforms in the C-terminal region where the alternate 4B exon provides a polylysine region in addition to posttranslational farnesylation. The other Ras isoforms lack the polylysine tail and are modified with a palmitoyl group in addition to the farnesyl moiety. Some of the unique properties of K-Ras4B have been revealed in studies of comparative physiology. These include induced Raf-1 activation in transfected cells (*7*), expression of matrix metalloproteinase 2 in fibroblasts (*8*), inhibition of apoptosis in stem cells (*9*), nucleolar localization and interaction with nucleolin in several cell types (*10*), and AKT activation and cell migration of fibroblasts in response to a growth factor (*11*). In the latter study, interaction of K-Ras4B with calmodulin (CaM)[1] was demonstrated and found to be necessary for the K-Ras4B-dependent growth factor responses.

In fact, CaM is the only protein found thus far to bind to K-Ras4B uniquely; the many other known binding partners interact with all four isoforms (*12*). Direct binding of CaM to K-Ras4B but not to the highly homologous H-Ras, N-Ras, or K-Ras4A has been demonstrated in fibroblasts (*13*), platelets and the MCF-7 breast cancer cell line (*14*), and Hela cells (*15*). This binding has also been demonstrated in a yeast two-hybrid assay (*14*). Functionally important consequences found for the K-Ras4B−CaM interaction include regulation of cell cycle through an ERK2 pathway (*16*), prevention of Ras activation by PKC in fibroblasts (*17*), and reversible intracellular translocation of K-Ras4B in hippocampal neurons in response to glutamate (*15*).

CaM is a ubiquitous $Ca^{2+}$-binding protein. Its dumbbell-like architecture is comprised of globular N- and C-terminal domains connected by a flexible linker. The general function of CaM is to mediate $Ca^{2+}$ signaling through interactions with numerous diverse CaM binding proteins. Calcium induces a conformational change in CaM rendering it competent for protein−protein interactions (*18*). CaM binding sites primarily contain basic and hydrophobic amino acids. In many cases the N- and C-terminal domains of CaM participate in intermolecular interactions and involve bending CaM into a globular structure (*19*).

†Supported by the American Cancer Society, Illinois Division Grant ACS 08-14 (to V.G.), and the U.S. Department of Health and Human Services.

*To whom correspondence should be addressed. Tel: 312-355-4965. Fax: 312-413-0353. E-mail: vadimg@uic.edu.

[1]Abbreviations: CaM, calmodulin; K-Ras4B$_{tr}$, K-Ras4B truncated (amino acid residues 1−166 only); HVR, hypervariable region; NMR, nuclear magnetic resonance; ITC, isothermal titration calorimetry; HSQC, heteronuclear single-quantum coherence.

© 2009 American Chemical Society
Published on Web 07/07/2009

Given the crucial role of K-Ras4B in oncogenesis, and the apparent uniqueness of its association with CaM, detailed understanding of the specifics of this interaction is essential and could lead to development of highly specific anticancer pharmaceutical agents. Currently, the precise role of K-Ras4B−CaM interaction in cancer is not well-defined. However, CaM clearly regulates K-Ras4B membrane association (*14*) that is crucial for K-Ras4B function in cancer. In addition, CaM binding to K-Ras4B activates AKT (*11*), a protein kinase hyperactivated in many cancer types. AKT plays a role in cell survival and resistance to cancer therapy (*20*, *21*). Phenotypically, AKT activation by K-Ras4B−CaM interaction results in increased cell migratory behavior that is characteristic of cells transformed by oncogenic K-Ras4B (*11*). There have been several reports on characterization of K-Ras4B−CaM interactions, with variable results. The binding event has been shown to have a strong dependence on $Ca^{2+}$, implying that K-Ras4B binds CaM in its $Ca^{2+}$-loaded form (*13*, *14*). CaM association with K-Ras4B was largely independent of the bound guanine nucleotide in the membranes of stimulated hippocampal neurons (*15*), but in cell-free assays CaM bound preferentially to the GTP-bound active form of K-Ras4B (*13*). A nanomolar dissociation constant for K-Ras4B−CaM binding was measured using surface plasmon resonance (*22*), while CaM antagonists with only micromolar affinity for CaM inhibited its binding to K-Ras4B (*15*, *23*).

Particularly variable results have been reported with regard to the domains of K-Ras4B that physically interact with CaM. The hypervariable region (HVR) at the C-terminal tail of K-Ras4B, expressed by itself in neurons, apparently bound CaM (*15*). However, in pull-down assays and surface plasmon resonance experiments the truncated glutathione *S*-transferase (GST) tagged catalytic domain (residues 1−166) of K-Ras4B also bound CaM (*13*, *22*), as did residues 1−166 of H-Ras (*13*) and the 151 amino acid sequence in an α-helix immediately adjacent to the HVR (*22*). On the other hand, a hemaglutinin (HA) tagged catalytic domain of K-Ras4B did not (*22*). CaM, with its extensive capacity to interact with a wide diversity of proteins, is a particularly promiscuous binding partner (*24*). It may be that interactions in cell-free systems with truncated and/or tagged peptides may include nonspecific associations.

Nuclear magnetic resonance (NMR) allows discernment of interaction patterns for individual amino acid residues and protein domains and thus is a good technique to study details of specific molecular interactions. Because NMR chemical shifts are sensitive to the rate of dissociation of weakly interacting molecules, it is possible to estimate the strength of protein−protein interactions and to define the binding interfaces. Addition of isothermal titration calorimetry (ITC) makes it possible to evaluate the energy of protein−protein interactions quantitatively. Using these approaches we demonstrate that the HVR of K-Ras4B is the primary binding site for CaM and is responsible for binding specificity. It interacts with the C-terminal domain and linker region of CaM with micromolar affinity. In addition, we show that the HVR peptide is unable to mimic completely the interactions between the full-length K-Ras4B and CaM. This observation suggests that the weak association with the catalytic domain of K-Ras4B is necessary for the higher affinity binding. The facts that the HVR constitutes the major binding site for CaM and that no CaM binding could be observed with the inactive GDP-bound K-Ras4B imply that the HVR may be influenced by the context of the full-length protein in the nucleotide-dependent manner.

## EXPERIMENTAL PROCEDURES

*Protein Expression, Purification, and Activity*. The full-length human K-Ras4B cDNA was purchased from Invitrogen and cloned into the pET42a bacterial expression vector using the *Nde*I and *Xho*I restriction sites, adding an N-terminal 6× histidine tag to ease protein purification. The plasmids were transformed into One Shot BL21-A1 cells (Invitrogen), grown overnight in LB media with kanamycin for antibiotic selection at 37 °C, and shaken at 250 rpm. For induction, the cells were diluted 1:20 into M9 media (with 0.4 M NaCl) and grown to an OD of 0.5−0.8 at 600 nm at 37 °C and 250 rpm. The cells were induced at 18 °C with 0.2 mM isopropyl β-D-1-thiogalactopyranoside (IPTG) and 0.2% arabinose in the presence of 2% ethanol and grown with shaking at 250 rpm for 22−28 h. We also found that K-Ras4B may also be produced at 37 °C in the absence of ethanol. Cells were harvested at 6000 rpm for 20 min at 4 °C in a GS-3 rotor. The supernatant was discarded, and the cell pellets were frozen at −80 °C. The cell pellets were lysed using B-PER bacterial extraction reagent (Pierce) with 10 mM $MgCl_2$, 50 μg/mL DNase I, 2 mM phenylmethanesulfonyl fluoride (PMSF), 1−2 tablets of EDTA-free Complete (Roche), and 10 mg of lysozyme. The cells were lysed for 20−30 min at room temperature on an orbital shaker. The lysates were centrifuged for 30 min at 18000 rpm in an SS34 rotor at 4 °C. The supernatant was collected, and GDP was added to 100 μM, sodium citrate to 20 mM, KCl to 50 mM, and β-mercaptoethanol to 5 mM. The solution was stirred for approximately 60 min. The pellets were resuspended in 10 mM Tris-HCl, pH 7.6, 20 mM sodium citrate, 50 mM KCl, 5 mM $MgCl_2$, 100 μM GDP, and 2 mM β-mercaptoethanol. The lysate was incubated on an orbital shaker for 30 min and then spun in a centrifuge the same way as the first lysate. Supernatants from both extractions were dialyzed against His-Bind 1× binding buffer (Novagen) with 10% glycerol overnight at 4 °C. For purification, each of the two extractions was incubated with $Ni^{2+}$-charged His-Bind resin (Novagen) for 2 h with gentle shaking. The slurry was transferred to a disposable column (Bio-Rad), and the column was washed extensively with 1× His-Bind binding buffer (no imidazole or glycerol), until no more protein was detectable by Bradford analysis. The column was washed with 1× His-Bind wash buffer (Novagen) containing 10 mM imidazole. Elutions were performed stepwise (60 mM, 100 mM, 200 mM, and 1 M imidazole). All fractions were analyzed on an SDS−PAGE gel. The purified protein was dialyzed into Tris−citrate buffer (50 mM Tris−citrate, pH 6.5, 50 mM NaCl, 5 mM $MgCl_2$, 10 mM β-mercaptoethanol, and 10 mM $CaCl_2$) for storage. For nucleotide loading, the protein solution was dialyzed into nucleotide loading buffer (25 mM Tris-HCl, pH 7.6, 150 mM NaCl, 10 mM $MgCl_2$, 5% glycerol, 1 mM EDTA, and 1 mM β-mercaptoethanol). Prior to the addition of GTP-γ-S to a final concentration of 0.1 mM, EDTA was added to a concentration of 10 mM to the protein solution. The reaction mix was incubated for 30 min at 30 °C. The reaction was stopped by adding $MgCl_2$ to a final concentration of 65 mM. Similar protocols were also used in the cloning and purification of truncated K-Ras4B (1−166) (K-Ras4B$_{tr}$).

To demonstrate the identity and activity of the purified protein, an enzymatic GTP hydrolysis assay and Raf-1 binding activity assay were performed. The hydrolysis assay was performed using the EnzChek phosphate assay kit (Invitrogen). Ras protein and GTP concentrations were 15 μM and 500 μM, respectively. Purine nucleoside phosphorylase (PNP) phosphorylates

2-amino-6-mercapto-7-methylpurine riboside (MESG) with the released phosphate causing an increase in absorbance at 360 nm. The reaction was monitored for 16 h using a Shimadzu spectrophotometer. Activity of GDP- and GTP-$\gamma$-S-loaded K-Ras4B proteins was also determined using Raf-1 Ras binding domain (RBD) agarose beads [Ras assay reagent (Raf-1 RBD agarose); Millipore]. The assay is based on the principle that GTP-$\gamma$-S-bound K-Ras4B undergoes a conformational change that allows it to bind to the RBD of Raf-1 while GDP-bound K-Ras4B does not. GTP-$\gamma$-S-bound and GDP-bound K-Ras4B proteins (200 ng) were added to 30 $\mu$L of Raf-1 RBD agarose beads and incubated in 500 $\mu$L of buffer containing 25 mM HEPES, pH 7.5, 1 mM EDTA, 10 mM $MgCl_2$, 1% NP-40, 0.25% sodium deoxycholate, 150 mM NaCl, and 10% glycerol. Proteinase inhibitors were added as follows just prior to use: 1 nM PMSF, 0.2 TIU aprotinin, 0.01 M NaF, and 0.2 mM sodium orthovanadate. Samples were incubated for 2 h at 4 °C on a tube rotator. Beads were then collected by a 30 s centrifugation at 14000*g* (Eppendorf 5415D). The supernatant was removed by aspiration, 400 $\mu$L of fresh buffer was added, and the centrifugation, rinsing, and aspiration were repeated three times. Thirty microliters of 2× Laemelli loading buffer was added to the beads, and the tube was heated to 80 °C for 13 min. Tubes were centrifuged as above, and 15 $\mu$L of supernatant was loaded onto a 12% polyacrylamide 1.0 mm thick bis-tris NuPage gel (Invitrogen). The gel was subjected to electrophoresis at 120 V for approximately 1.5 h and then electroblotted onto a PVDF membrane (Bio-Rad) at 30 V for 1.5 h. The blot was incubated in a primary K-Ras4B antibody (Ab-1; Oncogene Sciences) diluted 1:5000 in 3% milk in PBS-T (phosphate-buffered saline, pH 7.4, with 0.1% Tween 20) for 4 h at room temperature. After rinsing, the blot was treated with an anti-mouse secondary antibody coupled to horseradish peroxidase (GE Healthcare, U.K.) diluted 1:2000 in 3% milk in PBS-T. Bands were visualized by chemiluminescence using the ECL reagent kit (GE Healthcare) with photographic film. Western blots to show total K-Ras4B protein were done as above, except that 200 ng of each sample in Laemelli buffer was loaded directly onto the gel, without the use of the raf-1 RBD agarose beads.

Human CaM cDNA (Invitrogen) was cloned into the pET42a expression vector (Novagen). The protein was expressed in BL21-A1 *Escherichia coli* cells at 37 °C overnight after induction with 1 mM IPTG and 0.2% arabinose in M9 media containing $^{15}N$ and $^{13}C$ stable isotopes (Cambridge Isotope Laboratories). The cell pellets were resuspended in the equilibration buffer [10 mM Tris-HCl (pH 7.6), 10 mM $CaCl_2$, and 10 mM $\beta$-mercaptoethanol] and heated to 65 °C in a water bath for 30 min. The suspension was then centrifuged at 7000 rpm for 30 min. The supernatant was applied to a phenyl-Sepharose column preequilibrated in the equilibration buffer. The column was extensively washed with the equilibration buffer. The protein was eluted using elution buffer (10 mM Tris-HCl, pH 7.6, 5 mM EDTA, and 10 mM $\beta$-mercaptoethanol). The purity of the protein was assessed by SDS−PAGE electrophoresis. The pure fractions were pooled and concentrated. The CaM used in all experiments was $Ca^{2+}$ loaded.

*NMR Experiments*. The $^1H-^{15}N$ HSQC NMR experiments were performed on 600 and 800 MHz Bruker Avance spectrometers equipped with cryogenic probes. All experiments were carried out at 25 °C. The buffer conditions were as follows: 10% $D_2O$, 50 mM Tris−citrate (pH 6.5), 50 mM NaCl, 5 mM $MgCl_2$, 10 mM BME, and 10 mM $CaCl_2$. The CaM assignments were confirmed using CBCACONH, NHCA, and NHCACB experiments. All of the data were processed and analyzed using NMRPipe (*25*). The assignments were performed using Sparky (UCSF). For NMR titration experiments $^1H-^{15}N$ HSQC spectra were recorded at different $^{15}N$ CaM:K-Ras4B/K-Ras4B$_{tr}$/HVR molar ratios. The mean chemical shift difference ($\Delta\delta_{NH}$) of the $^1H$ and $^{15}N$ nuclei was calculated as previously described (*26*):

$$\Delta\delta_{NH} = \sqrt{\frac{(\Delta\delta H_N)^2+(\Delta\delta N)^2/25}{2}}$$

The chemical shift changes above average plus one standard deviation were considered statistically significant as commonly done in NMR studies.

*ITC Experiments*. K-Ras4B-GTP-$\gamma$-S, the HVR peptide, K-Ras4B$_{tr}$-GTP-$\gamma$-S, K-Ras4B-GDP, and CaM were dialyzed into a buffer consisting of 50 mM Tris−citrate, pH 6.5, 50 mM NaCl, 5 mM $MgCl_2$, 1 mM tris(2-carboxyethyl)phosphine hydrochloride (TCEP), and 10 mM $CaCl_2$. The titration experiments were performed using a VP-ITC microcalorimeter (MicroCal LLC, Northampton, MA) at 25 °C. For the titration, 25−27 aliquots (10 $\mu$L each) of 1 mM CaM were injected into the ITC cell containing 1.4 mL of 70 $\mu$M K-Ras4B-GTP-$\gamma$-S, the HVR peptide, K-Ras4B$_{tr}$-GTP-$\gamma$-S, or K-Ras-GDP. Each titration was preceded by a single 2 $\mu$L injection to eliminate the diffusion artifacts. A reference titration was run, with only buffer in the cell instead of K-Ras4B proteins or the HVR, to offset thermodynamic effects of protein dilution. The reference data were subtracted from the protein titration data points. The initial 2 $\mu$L titration point was discarded. The integrated heat values were analyzed using the "Origin 7.0" software as well as the Scientist 3.0 software (Micromath Scientific Software). The data were fit using the "one set of sites" model to yield the dissociation constant ($K_d$), the molar ratio, and other thermodynamic parameters.

## RESULTS

*Recombinant K-Ras4B and K-Ras4B$_{tr}$ Are Biologically Active*. The first requirement for investigation of relevant protein−protein interactions between K-Ras4B and CaM is the availability of biologically active proteins. Since the ability to produce recombinant K-Ras4B protein has been established in many laboratories including our own, here we concentrate on testing the activity of K-Ras4B. First, we tested the ability of K-Ras4B and K-Ras4B$_{tr}$ proteins to interact with the Ras binding domain (RDB) of Raf-1. The Raf-1 RBD binding test is commonly used to assess K-Ras4B activity and is based on the principle that GTP-bound Ras undergoes a conformational change that allows it to bind to the Raf-1 RBD (*27*). Western blots in Figure 1A show that both K-Ras4B and K-Ras4B$_{tr}$, when bound to GTP-$\gamma$-S, were able to bind Raf-1 RBD with high affinity, while the GDP-loaded negative controls exhibited weak binding (12−15% band intensity of GTP-$\gamma$-S-loaded K-Ras4B as measured by gel scanning). These results are consistent with the literature reports showing that GTP-bound Ras binds Raf-1 RBD with high affinity, while GDP-loaded Ras displays low micromolar affinity toward Raf-1 RBD (*28*). Alternatively, the samples of GDP-loaded K-Ras4B may have contained a trace amount of GTP-bound protein. However, in our preparations of $^{15}N$ K-Ras4B-GDP using the same nucleotide loading procedure we did not observe signals corresponding to K-Ras4B-GTP in $^1H-^{15}N$ HSQC NMR experiments. Four separate K-Ras4B

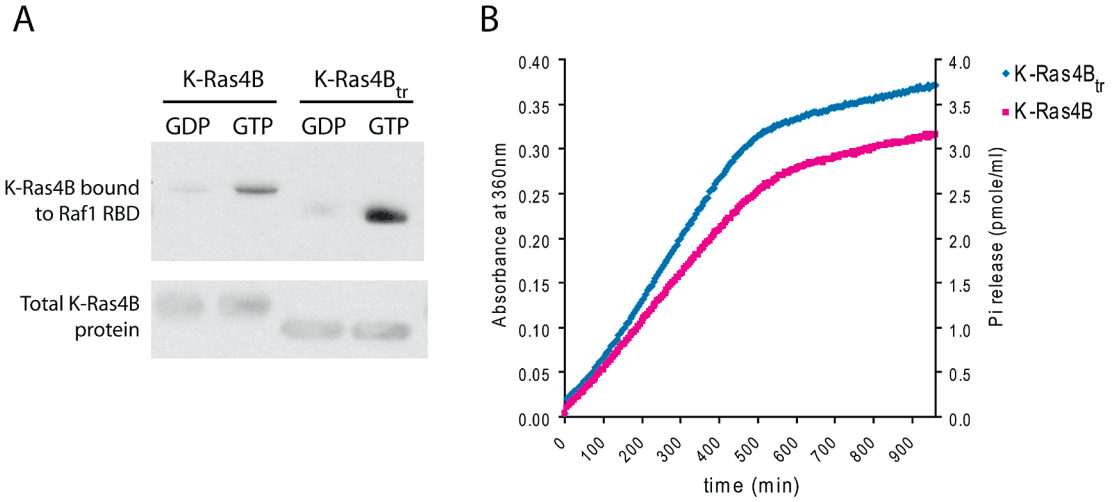


FIGURE 1: (A) Western blot showing the Raf-1 RBD binding activity of recombinant K-Ras4B and K-Ras4B$_{tr}$. The GDP-bound K-Ras4B and K-Ras4B$_{tr}$ do not bind the RBD of Raf-1, but the GTP-bound form of the proteins binds the RBD of Raf-1, indicative of protein activity. (B) Enzymatic activity of K-Ras4B and K-Ras4B$_{tr}$ proteins was tested by measuring GTP hydrolysis rates using the EnzChek phosphate assay kit (Invitrogen). Recombinant K-Ras4B and K-Ras4B$_{tr}$ proteins are able to hydrolyze GTP, indicating that they are enzymatically active.

activity assays were performed to establish a linear range for the GTP-$\gamma$-S samples, all with similar results (data not shown). The data presented here demonstrate that recombinant K-Ras4B and K-Ras4B$_{tr}$ proteins were both Raf-1 binding competent.

Next, the ability of K-Ras4B and K-Ras4B$_{tr}$ to hydrolyze GTP was tested in a GTP hydrolysis assay. The results shown in Figure 1B represent a typical time course for GTP hydrolysis (*29*) and indicate that both K-Ras4B and K-Ras4B$_{tr}$ are able to hydrolyze GTP. The determined initial rates of GTP hydrolysis measured at the same protein concentration were 51.03 and 67.56 pmol/min for K-Ras4B and K-Ras4B$_{tr}$, respectively. The 32% difference in rates of GTP hydrolysis between K-Ras4B and K-Ras4B$_{tr}$ is in agreement with previously published results (*30*). Together, we demonstrate that recombinant K-Ras4B and K-Ras4B$_{tr}$ are both enzymatically active and Raf-1 binding competent.

*The N- and C-Terminal Domains of CaM Define the Interaction Sites with K-Ras4B*. Upon titration of K-Ras4B loaded with GTP-$\gamma$-S into a 0.15 mM solution of $^{15}$N CaM significant K-Ras4B concentration-dependent chemical shift changes in the signals of CaM were observed in NMR $^{1}$H$-^{15}$N heteronuclear single-quantum coherence (HSQC) experiments (Figure 2A). The fact that the titration produced chemical shift changes as illustrated in Figure 2B indicates fast exchange on the NMR time scale. The fast exchange phenomenon is observed when the binding affinity is relatively low, allowing rapid interconversion between the free and the bound species. Analysis of chemical shift perturbations indicates that the most significant chemical shift changes induced by K-Ras4B-GTP-$\gamma$-S occur in the regions comprising residues A15, T29, L32, L48, I52, and E67 in the N-terminal $\beta$-sheet region, residues D78 and T79 in the linker region, and the C-terminal F92, R106, M109−N111, and Q143−M145 residues of CaM (Figure 2C). Mapping of chemical shift perturbations onto the structure of CaM (*31*) revealed that the K-Ras4B-GTP-$\gamma$-S binding interface includes the N- and C-terminal domains and the linker region (Figure 2D).

*The HVR of K-Ras4B Provides Specificity for K-Ras4B Binding to CaM*. To test if the HVR of K-Ras4B binds to CaM, a 22 amino acid synthetic peptide representing the HVR of K-Ras4B was purchased from Biopeptide, Inc. Titration of $^{15}$N CaM with the HVR peptide was followed by $^{1}$H$-^{15}$N HSQC spectra recorded on the peptide−protein mixtures at different molar ratios. The overlay of spectra for $^{15}$N CaM alone and $^{15}$N CaM saturated with the HVR peptide is shown in Figure 3A. Similar to the K-Ras4B-GTP-$\gamma$-S binding to CaM, the fast exchange phenomenon indicative of low-affinity binding was observed in NMR titration experiments (Figure 3B). Addition of the HVR peptide induced significant chemical shift changes in the linker region (residues D78, T79, E82−E84) and the C-terminal domain of CaM (residues F92, D93, R106, M109, T110, G113, E123, D129, M144, A147, and K148) (Figure 3C). Only limited chemical shift perturbations are observed in the N-terminal domain of CaM in residues I63 and F68, presumably due to their proximity to the linker region. Mapping of chemical shift perturbations onto the structure of CaM (Figure 3D) indicates that the binding interface is primarily comprised of negatively charged amino acids in the linker region and those flanking the hydrophobic pockets in CaM, such as D78, E82, E84, D93, and D129. Thus, the HVR of K-Ras4B can directly participate in specific interactions with CaM.

To test whether the catalytic domain of K-Ras4B is involved in binding CaM, we performed an NMR titration of $^{15}$N CaM with K-Ras4B$_{tr}$ loaded with GTP-$\gamma$-S (Figure 4A). The presence of fast chemical exchange indicates weak binding of K-Ras4B$_{tr}$ to CaM (Figure 4B). The binding interface in CaM involves small areas in both the N- and C-terminal domains comprised of residues T5, I27, T28, L32, A57, and E67 in the N-terminal domain and residues F92, R106, M109, and N111 in the C-terminal domain (Figure 4C,D). Binding involves predominantly nonpolar and hydrophobic amino acids. Together, the results of these experiments delineate the K-Ras4B−CaM binding interface. While the HVR may preferentially bind to the C-terminal domain of CaM, the catalytic domain of K-Ras4B alone weakly binds to both the N- and C-terminal domains.

*The HVR of K-Ras4B May Contain the Major CaM Binding Site*. To further investigate the contributions of K-Ras4B domains to binding CaM, we measured dissociation constants using ITC experiments. Consistent with our NMR data, K-Ras4B loaded with GTP-$\gamma$-S and the HVR of K-Ras4B bound CaM with low micromolar affinity. Endothermic binding is observed for K-Ras4B and the HVR as judged by the sign of the heat of the reaction. K-Ras4B-GTP-$\gamma$-S bound CaM with 1:1

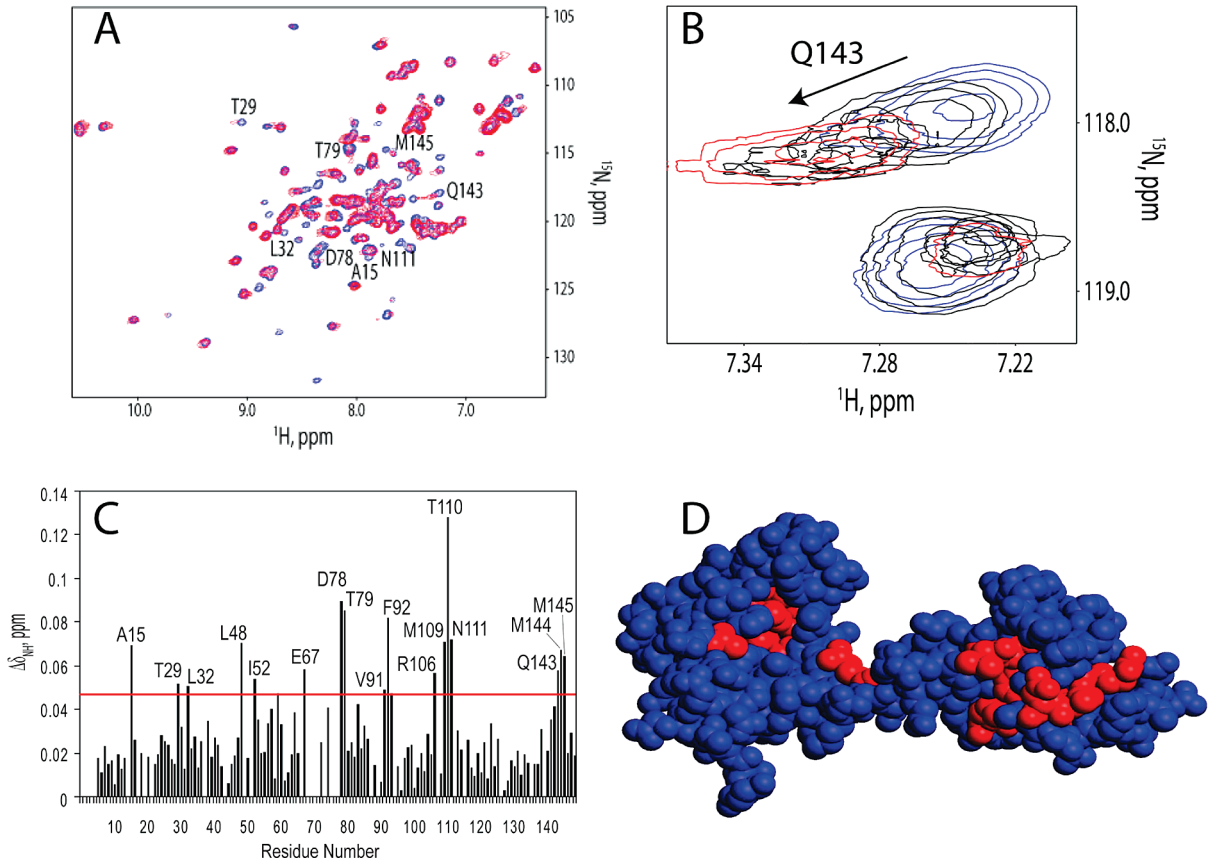


FIGURE 2: (A) A superimposition of $^1$H−$^{15}$N HSQC spectra of 150 $\mu$M $^{15}$N CaM (blue) and $^{15}$N CaM bound to 2 mol equiv of GTP-$\gamma$-S-loaded K-Ras4B (red). The spectra were acquired at 600 MHz at 25 °C with 128 indirect points. The buffer conditions are 50 mM Tris−citrate (pH 6.5), 50 mM NaCl, 5 mM $MgCl_2$, 10 mM BME, and 10 mM $CaCl_2$. Examples of resonances that shift significantly in response to K-Ras4B binding are indicated. (B) A zoom of the resonance belonging to Q143 shows the progressive shift of the peak with no addition of GTP-$\gamma$-S-loaded K-Ras4B (blue) to the saturation point with 2 mol equiv of GTP-$\gamma$-S-loaded K-Ras4B (red). Intermediate titration points with the addition of 0.25, 0.5, and 1 mol equiv of GTP-$\gamma$-S-loaded K-Ras4B are shown in black. (C) Plot of chemical shift changes using the weighted average of $^1$H and $^{15}$N resonance frequencies versus the residue number in the sequence of CaM from the N- to the C-terminus. Residues that show statistically significant chemical shift changes (average plus one standard deviation indicated by the red line) are marked. (D) Model of CaM structure showing the regions that interact with GTP-$\gamma$-S-loaded K-Ras4B. Residues that show statistically significant chemical shift changes with the addition of 2 mol equiv of GTP-$\gamma$-S-loaded K-Ras4B are shown in red.

stoichiometry (Figure 5A) with a dissociation constant ($K_d$) of 3.4 ± 1.2 $\mu$M. The other fitted parameters were $\Delta H$ = 2.5 ± 0.8 kcal/mol and $\Delta S$ = 30.5 cal deg$^{-1}$ mol$^{-1}$. In the case of the HVR peptide titrated with CaM (Figure 5B), the titration curve was fit to the "one set of binding sites" model yielding a dissociation constant of $K_d$ = 11.2 ± 1.6 $\mu$M, $\Delta H$ = 0.65 ± 0.1 kcal/mol, and $\Delta S$ = 25.1 cal deg$^{-1}$ mol$^{-1}$. The fit revealed one binding site for the HVR peptide on CaM. Initially, K-Ras4B interaction with CaM was reported to be nucleotide independent (*15*). However, subsequent reports demonstrated a strong preference for GTP-bound K-Ras4B by CaM (*13*, *22*). To test the nucleotide dependence of K-Ras4B binding to CaM, we performed an ITC experiment with K-Ras4B-GDP and CaM. Consistent with literature reports (*13*), ITC experiments for GDP-bound K-Ras4B showed no significant binding (Figure 5C).

In addition to the determination of dissociation constants by ITC, we obtained corroborating results using nonlinear regression analysis of concentration-dependent NMR chemical shift perturbations. Chemical shift perturbations for five amino acids in CaM responding to titration with either K-Ras4B-GTP-$\gamma$-S, K-Ras4B$_{tr}$-GTP-$\gamma$-S, or the HVR peptide were used in the fitting procedure. Examples of these fits are shown in Figure 6. While saturation with K-Ras4B-GTP-$\gamma$-S and the HVR peptide occurs between 1:1.5 to 1:2 molar ratio (Figure 6A,C), saturation with K-Ras4B$_{tr}$-GTP-$\gamma$-S occurs at around 1:8 molar ratio (Figure 6B) and is indicative of a much weaker binding affinity. The corresponding dissociation constant ($K_d$) values are 7.2 ± 4.2, 17.5 ± 10.1, and 307.6 ± 122.3 $\mu$M for K-Ras4B-GTP-$\gamma$-S, the HVR peptide, and K-Ras4B$_{tr}$GTP-$\gamma$-S, respectively. The dissociation constants ($K_d$) obtained for K-Ras4B-GTP-$\gamma$-S and the HVR peptide binding to CaM from NMR titration experiments are not statistically different from those obtained by ITC. Due to the very weak binding affinity, we could not use ITC to measure the dissociation constant for the K-Ras4B$_{tr}$-GTP-$\gamma$-S−CaM binding. However, since the dissociation constant ($K_d$) values measured using NMR titration and ITC are in agreement, we could use the $K_d$ value determined using NMR titration to estimate binding affinity of CaM to K-Ras4B$_{tr}$-GTP-$\gamma$-S.

In conclusion, both the HVR and the GTP-$\gamma$-S-loaded catalytic domain of K-Ras4B contribute to CaM binding affinity with the HVR providing the major binding site. Interactions between K-Ras4B and CaM are significantly weaker upon loading with GDP. Since K-Ras4B-GDP exhibits little or no binding affinity for CaM as compared to the HVR, we propose that interactions between the HVR and the catalytic domain of K-Ras4B-GDP may sequester the HVR to prevent it from binding CaM or alter its structure.

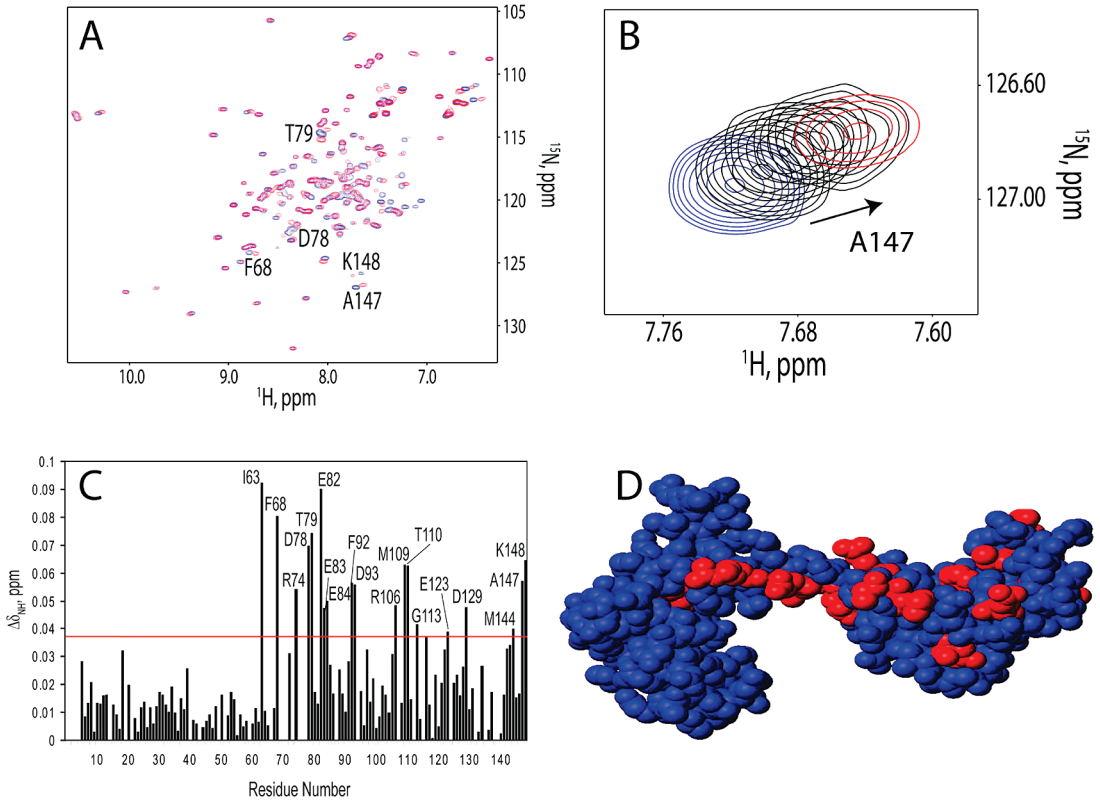


FIGURE 3: (A) A superimposition of $^1$H−$^{15}$N HSQC spectra of 136 $\mu$M $^{15}$N CaM (blue) and $^{15}$N CaM bound to 2.1 mol equiv of the HVR peptide (red). The spectra were acquired at 600 MHz at 25 °C with 128 indirect points. The buffer conditions are 50 mM Tris−citrate (pH 6.5), 50 mM NaCl, 5 mM $MgCl_2$, 10 mM BME, and 10 mM $CaCl_2$. Examples of resonances that shift significantly in response to HVR peptide binding are indicated. (B) A zoom of the resonance belonging to A147 shows the progressive shift of the peak with no addition of the HVR peptide (blue) to the saturation point with 2.1 mol equiv of the HVR peptide (red). Intermediate titration points with the addition of 0.26, 0.53, 1.1, and 1.6 mol equiv of the HVR peptide are shown in black. (C) Plot of chemical shift changes using the weighted average of $^1$H and $^{15}$N resonance frequencies versus the residue number in the sequence of CaM from the N- to the C-terminus. Residues that show statistically significant chemical shift changes (average plus one standard deviation indicated by the red line) are marked. (D) Model of the CaM structure showing the regions that interact with the HVR peptide. Residues that show statistically significant chemical shift changes with the addition of 2.1 mol equiv of the HVR peptide are shown in red.

## DISCUSSION

Our results suggest that specific binding of K-Ras4B to CaM occurs through the unique HVR and show that CaM interacts with nonfarnesylated human K-Ras4B with micromolar affinity. The apparent disagreement of this result with the previously measured nanomolar affinity by surface plasmon resonance of the GST-tagged K-Ras4B catalytic domain for CaM may be explained by differences in protein constructs and experimental approaches (*22*). The K-Ras4B binding site on CaM resides in the N- and C-terminal domains (Figure 2). Both the HVR and the GTP-$\gamma$-S-loaded catalytic domain are involved in interaction with CaM.

Binding the HVR peptide and K-Ras4B$_{tr}$-GTP-$\gamma$-S to the C-terminal domain of CaM involves the same regions, namely, residues F92 and D93 and the R106, M109−N111 region (Figures 3 and 4). This suggests that either the HVR or the catalytic domain of K-Ras4B may interact with the C-terminal domain of CaM. However, due to its higher binding affinity, the HVR may predominantly interact with the linker region and the C-terminal domain of CaM (Figures 5 and 6), while the GTP-$\gamma$-S-loaded catalytic domain (1−166) of K-Ras4B may bind the N-terminal domain of CaM. Specific binding of the highly positively charged HVR to the linker region and the C-terminal domain is justified by the fact that the negatively charged residues concentrate in the C-terminal domain of CaM, while the N-terminal domain presents a mixture of negative and positive charges. Specific interaction of a positively charged peptide with the C-terminal domain of CaM has been observed in the structure of the CaM−CaMKIIa complex (*32*). We hypothesize that the farnesyl group on the C-terminus of the HVR may further enhance the binding affinity of K-Ras4B for CaM through interactions with the hydrophobic residues in the C-terminal domain of CaM. The importance of K-Ras4B farnesylation for binding to CaM has been previously demonstrated (*15*, *22*).

Binding of the K-Ras4B catalytic domain to the N-terminal domain of CaM is also not conventional. Instead of employing the binding interfaces commonly found in CaM which includes the methionine-lined hydrophobic patch, the catalytic domain of K-Ras4B interacts with hydrophobic I27−L32 (spanning the $\beta$1-strand of the central $\beta$-sheet and the beginning of the $\alpha$2-helix) and L48−I52 (part of the $\alpha$3-helix) regions. This is consistent with the involvement of the hydrophobic helix 5 region of the catalytic domain of K-Ras4B in binding CaM (*22*). The apparent binding to CaM of the hydrophobic $\alpha$-helix 5 peptide (amino acids 151−166) when independently expressed may indicate that this region participates in binding when in the context of the full-length protein and/or enhances the binding of the HVR (*22*). Identification of chemical shift perturbations in negatively charged E67 of CaM upon binding K-Ras4B is indicative of possible electrostatic contributions to CaM interactions with the catalytic domain of K-Ras4B. Participation of positively charged

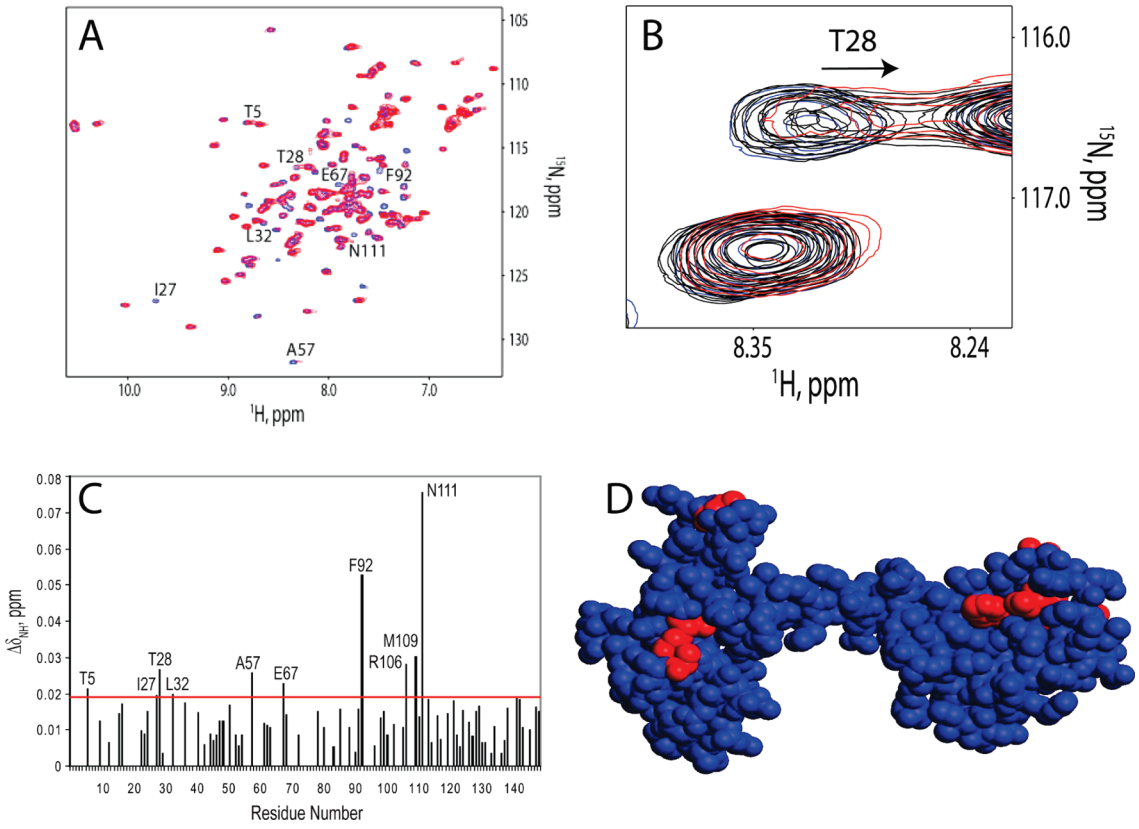


FIGURE 4: (A) A superimposition of $^{1}$H−$^{15}$N HSQC spectra of 150 $\mu$M $^{15}$N CaM (blue) and $^{15}$N CaM bound to 8 mol equiv of GTP-$\gamma$-S-loaded K-Ras4B$_{tr}$ (red). The spectra were acquired at 600 MHz at 25 °C with 128 indirect points. The buffer conditions are 50 mM Tris−citrate (pH 6.5), 50 mM NaCl, 5 mM $MgCl_2$, 10 mM BME, and 10 mM $CaCl_2$. Examples of resonances that shift significantly in response to K-Ras4B$_{tr}$ binding are indicated. (B) A zoom of the resonance belonging to T28 showing the progressive shift of the peak with no addition of GTP-$\gamma$-S-loaded K-Ras4B$_{tr}$ (blue) to the saturation point with 8 mol equiv of GTP-$\gamma$-S-loaded K-Ras4B$_{tr}$ (red). Intermediate titration points with the addition of 0.5, 1, 2, and 4 mol equiv of GTP-$\gamma$-S-loaded K-Ras4B$_{tr}$ are shown in black. (C) Plot of chemical shift changes using the weighted average of $^{1}$H and $^{15}$N resonance frequencies versus the residue number in the sequence of CaM from the N- to the C-terminus. Residues that show statistically significant chemical shift changes (average plus one standard deviation indicated by the red line) are marked. (D) Model of the CaM structure showing the regions that interact with GTP-$\gamma$-S-loaded K-Ras4B$_{tr}$. Residues that show statistically significant chemical shift changes with the addition of 8 mol equiv of GTP-$\gamma$-S-loaded K-Ras4B$_{tr}$ are shown in red.

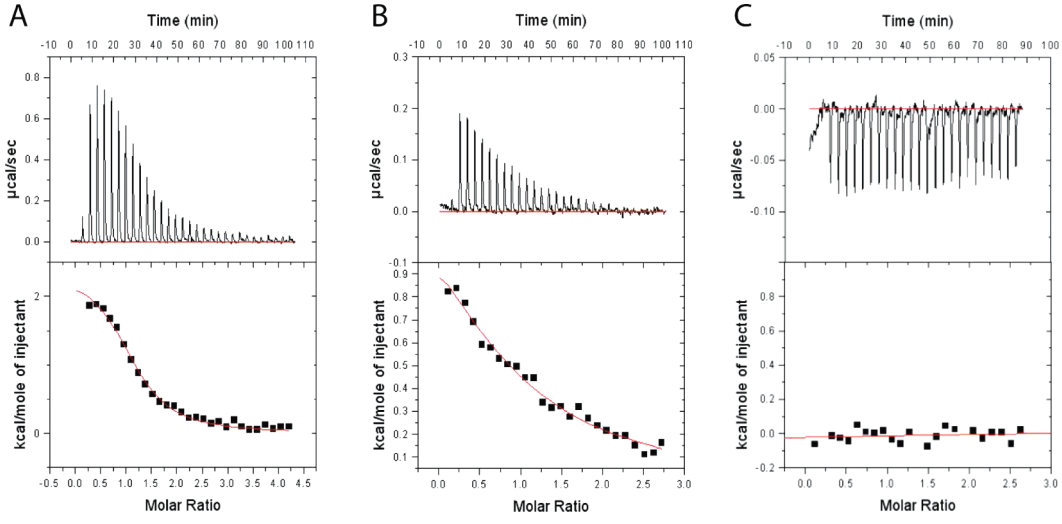


FIGURE 5: ITC titration of (A) 70 $\mu$M full-length K-Ras4B-GTP-$\gamma$-S with 1 mM CaM, (B) 70 $\mu$M HVR with 1 mM CaM, and (C) 70 $\mu$M K-Ras4B-GDP with 1 mM CaM. The upper panels in (A), (B), and (C) show titration isotherms. The lower panels in (A), (B), and (C) show the fit of the reference-subtracted titration data varying the number of sites ($N$), $K_d$, $\Delta H$, and $\Delta S$ parameters in the "one set of binding sites" model.

R68 and R73 from the switch II region of K-Ras4B in the CaM binding interface was recently discovered using point mutagenesis experiments (*22*).

The parallel arrangement of interacting partners in the K-Ras4B−CaM complex is an unusual way of binding CaM. It significantly differs from the common CaM binding mode that

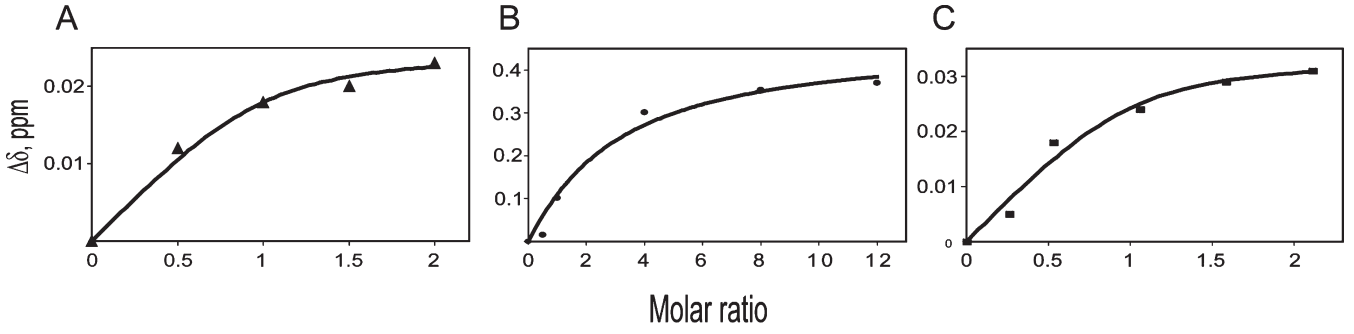


FIGURE 6: Examples of nonlinear fits for chemical shift perturbations in CaM responding to titration with (A) GTP-$\gamma$-S-loaded K-Ras4B, (B) GTP-$\gamma$-S-loaded K-Ras4B$_{tr}$, and (C) the HVR peptide. Both K-Ras4B-GTP-$\gamma$-S and the HVR peptide show saturation between 1.5 and 2 mol equiv while K-Ras4B$_{tr}$-GTP-$\gamma$-S shows saturation only at 8 mol equiv.

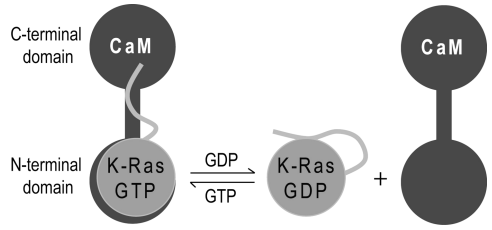


FIGURE 7: Hypothetical model showing the role of the HVR in the interaction of K-Ras4B with CaM. When GTP is bound to the catalytic domain, the HVR of K-Ras4B interacts specifically with the C-terminal domain and the linker region of CaM, while the catalytic domain (1−166) interacts with the N-terminal domain, giving a parallel binding pattern. When GDP is bound to the catalytic domain (1−166), the HVR would be sequestered, thereby preventing the interaction with CaM.

involves bending of the linker region to accommodate the hydrophobic pockets in the N- and C-terminal domains forming one extensive interface with the target (*18*, *19*). Parallel binding modes have been previously observed in the complex of CaM with the hydrophobic IQ domain of the cardiac $Ca_V1.2$ calcium channel (*33*) and in the complex of CaM with CaM-dependent kinase kinase peptide (*34*).

Although the HVR is a major CaM binding site, in the context of GDP-loaded K-Ras4B it is unable to efficiently interact with CaM. We hypothesize that the HVR is modulated by the K-Ras4B catalytic domain in a nucleotide-dependent manner. Our model that shows how the HVR may be involved in nucleotide-dependent binding to CaM is depicted in Figure 7. In the GDP-bound state the HVR may be sequestered by the catalytic domain of K-Ras4B while GTP binding induces a conformational change that may release the HVR from the catalytic domain and make it available to interact with CaM. Farnesylation at the C-terminus of the HVR of K-Ras4B may further enhance this mechanism by increasing the affinity of the HVR for the GDP-bound catalytic domain. This model is consistent with all of our data and currently available literature reports. For example, the HVR of H-Ras has been shown to transiently interact with the catalytic domain of H-Ras (*26*). However, further testing of the proposed mechanism of K-Ras4B engagement in protein−protein interactions is required.

In conclusion, we show that nonfarnesylated GTP-$\gamma$-S-loaded K-Ras4B interacts with both the N- and C-terminal domains of CaM with micromolar affinity. The HVR of K-Ras4B provides specificity and most of the affinity for this interaction. While the role of the HVR of K-Ras4B as a membrane anchor is well documented, its participation in protein−protein interactions is not yet fully explored. Since the HVR of K-Ras4B mediates specific interactions with CaM, it is possible that it modulates binding to other proteins in a specific manner. Thus, in addition to targeting of K-Ras4B to unique membrane compartments the HVR may also achieve specificity of K-Ras4B signaling by its involvement in protein−protein interactions.

## REFERENCES

1. Barbacid, M. (1987) ras genes. *Annu. Rev. Biochem. 56*, 779–827.
2. Kumar, R., Sukumar, S., and Barbacid, M. (1990) Activation of ras oncogenes preceding the onset of neoplasia. *Science* (*New York*) *248*, 1101–1104.
3. Malkinson, A. M. (1992) Primary lung tumors in mice: an experimentally manipulable model of human adenocarcinoma. *Cancer Res. 52*, 2670s–2676s.
4. Meuwissen, R., Linn, S. C., van der Valk, M., Mooi, W. J., and Berns, A. (2001) Mouse model for lung tumorigenesis through Cre/lox controlled sporadic activation of the K-Ras oncogene. *Oncogene 20*, 6551–6558.
5. Janssen, K. P., el-Marjou, F., Pinto, D., Sastre, X., Rouillard, D., Fouquet, C., Soussi, T., Louvard, D., and Robine, S. (2002) Targeted expression of oncogenic K-ras in intestinal epithelium causes spontaneous tumorigenesis in mice. *Gastroenterology 123*, 492–504.
6. Carta, C., Pantaleoni, F., Bocchinfuso, G., Stella, L., Vasta, I., Sarkozy, A., Digilio, C., Palleschi, A., Pizzuti, A., Grammatico, P., Zampino, G., Dallapiccola, B., Gelb, B. D., and Tartaglia, M. (2006) Germline missense mutations affecting KRAS isoform B are associated with a severe Noonan syndrome phenotype. *Am. J. Hum. Genet. 79*, 129–135.
7. Voice, J. K., Klemke, R. L., Le, A., and Jackson, J. H. (1999) Four human ras homologs differ in their abilities to activate Raf-1, induce transformation, and stimulate cell motility. *J. Biol. Chem. 274*, 17164–17170.
8. Liao, J., Wolfman, J. C., and Wolfman, A. (2003) K-ras regulates the steady-state expression of matrix metalloproteinase 2 in fibroblasts. *J. Biol. Chem. 278*, 31871–31878.
9. Plowman, S. J., Berry, R. L., Bader, S. A., Luo, F., Arends, M. J., Harrison, D. J., Hooper, M. L., and Patek, C. E. (2006) K-ras 4A and 4B are co-expressed widely in human tissues, and their ratio is altered in sporadic colorectal cancer. *J. Exp. Clin. Cancer Res. 25*, 259–267.
10. Birchenall-Roberts, M. C., Fu, T., Kim, S. G., Huang, Y. K., Dambach, M., Resau, J. H., and Ruscetti, F. W. (2006) K-Ras4B proteins are expressed in the nucleolus: Interaction with nucleolin. *Biochem. Biophys. Res. Commun. 348*, 540–549.
11. Liao, J., Planchon, S. M., Wolfman, J. C., and Wolfman, A. (2006) Growth factor-dependent AKT activation and cell migration requires the function of c-K(B)-Ras versus other cellular ras isoforms. *J. Biol. Chem. 281*, 29730–29738.
12. Rodriguez-Viciana, P., Sabatier, C., and McCormick, F. (2004) Signaling specificity by Ras family GTPases is determined by the full spectrum of effectors they regulate. *Mol. Cell. Biol. 24*, 4943–4954.
13. Villalonga, P., Lopez-Alcala, C., Bosch, M., Chiloeches, A., Rocamora, N., Gil, J., Marais, R., Marshall, C. J., Bachs, O., and Agell, N. (2001) Calmodulin binds to K-Ras, but not to H- or N-Ras, and modulates its downstream signaling. *Mol. Cell. Biol. 21*, 7345–7354.

14. Sidhu, R. S., Clough, R. R., and Bhullar, R. P. (2003) $Ca^{2+}$/calmodulin binds and dissociates K-RasB from membrane. *Biochem. Biophys. Res. Commun. 304*, 655–660.
15. Fivaz, M., and Meyer, T. (2005) Reversible intracellular translocation of KRas but not HRas in hippocampal neurons regulated by $Ca^{2+}$/calmodulin. *J. Cell Biol. 170*, 429–441.
16. Bosch, M., Gil, J., Bachs, O., and Agell, N. (1998) Calmodulin inhibitor W13 induces sustained activation of ERK2 and expression of p21(cip1). *J. Biol. Chem. 273*, 22145–22150.
17. Villalonga, P., Lopez-Alcala, C., Chiloeches, A., Gil, J., Marais, R., Bachs, O., and Agell, N. (2002) Calmodulin prevents activation of Ras by PKC in 3T3 fibroblasts. *J. Biol. Chem. 277*, 37929–37935.
18. Trewhella, J. (1992) The solution structures of calmodulin and its complexes with synthetic peptides based on target enzyme binding domains. *Cell Calcium 13*, 377–390.
19. Ikura, M., Clore, G. M., Gronenborn, A. M., Zhu, G., Klee, C. B., and Bax, A. (1992) Solution structure of a calmodulin-target peptide complex by multidimensional NMR. *Science* (*New York*) *256*, 632–638.
20. Qiao, M., Sheng, S., and Pardee, A. B. (2008) Metastasis and AKT activation. *Cell Cycle* (*Georgetown, TX*) *7*, 2991–2996.
21. Steelman, L. S., Stadelman, K. M., Chappell, W. H., Horn, S., Basecke, J., Cervello, M., Nicoletti, F., Libra, M., Stivala, F., Martelli, A. M., and McCubrey, J. A. (2008) Akt as a therapeutic target in cancer. *Expert Opin. Ther. Targets 12*, 1139–1165.
22. Lopez-Alcala, C., Alvarez-Moya, B., Villalonga, P., Calvo, M., Bachs, O., and Agell, N. (2008) Identification of essential interacting elements in K-Ras/calmodulin binding and its role in K-Ras localization. *J. Biol. Chem. 283*, 10621–10631.
23. Hidaka, H., Sasaki, Y., Tanaka, T., Endo, T., Ohno, S., Fujii, Y., and Nagata, T. (1981) N-(6-aminohexyl)-5-chloro-1-naphthalenesulfonamide, a calmodulin antagonist, inhibits cell proliferation. *Proc. Natl. Acad. Sci. U.S.A. 78*, 4354–4357.
24. Clapham, D. E. (2007) Calcium signaling. *Cell 131*, 1047–1058.
25. Delaglio, F., Grzesiek, S., Vuister, G. W., Zhu, G., Pfeifer, J., and Bax, A. (1995) NMRPipe: a multidimensional spectral processing system based on UNIX pipes. *J. Biomol. NMR 6*, 277–293.
26. Thapar, R., Williams, J. G., and Campbell, S. L. (2004) NMR characterization of full-length farnesylated and non-farnesylated H-Ras and its implications for Raf activation. *J. Mol. Biol. 343*, 1391–1408.
27. de Rooij, J., and Bos, J. L. (1997) Minimal Ras-binding domain of Raf1 can be used as an activation-specific probe for Ras. *Oncogene 14*, 623–625.
28. Herrmann, C., Martin, G. A., and Wittinghofer, A. (1995) Quantitative analysis of the complex between p21ras and the Ras-binding domain of the human Raf-1 protein kinase. *J. Biol. Chem. 270*, 2901–2905.
29. Schlichting, I., Rapp, G., John, J., Wittinghofer, A., Pai, E. F., and Goody, R. S. (1989) Biochemical and crystallographic characterization of a complex of c-Ha-ras p21 and caged GTP with flash photolysis. *Proc. Natl. Acad. Sci. U.S.A. 86*, 7687–7690.
30. John, J., Schlichting, I., Schiltz, E., Rosch, P., and Wittinghofer, A. (1989) C-terminal truncation of p21H preserves crucial kinetic and structural properties. *J. Biol. Chem. 264*, 13086–13092.
31. Chattopadhyaya, R., Meador, W. E., Means, A. R., and Quiocho, F. A. (1992) Calmodulin structure refined at 1.7 Å resolution. *J. Mol. Biol. 228*, 1177–1192.
32. Wall, M. E., Clarage, J. B., and Phillips, G. N. (1997) Motions of calmodulin characterized using both Bragg and diffuse X-ray scattering. *Structure 5*, 1599–1612.
33. Fallon, J. L., Halling, D. B., Hamilton, S. L., and Quiocho, F. A. (2005) Structure of calmodulin bound to the hydrophobic IQ domain of the cardiac Ca(v)1.2 calcium channel. *Structure 13*, 1881–1886.
34. Osawa, M., Tokumitsu, H., Swindells, M. B., Kurihara, H., Orita, M., Shibanuma, T., Furuya, T., and Ikura, M. (1999) A novel target recognition revealed by calmodulin in complex with $Ca^{2+}$-calmodulin-dependent kinase kinase. *Nat. Struct. Biol. 6*, 819–824.